Available online at www.sciencedirect.com
ScienceDirect
International Journal of Heat and Mass Transfer 51 (2008) 1313–1324
International Journal of HEAT and MASS TRANSFER
www.elsevier.com/locate/ijhmt

Droplet heat and mass transfer in a turbulent hot airstream

Maher M. Abou Al-Sood, Madjid Birouk *

Department of Mechanical and Manufacturing Engineering, University of Manitoba, Winnipeg, Manitoba, Canada R3T 5V6

Received 8 May 2007; received in revised form 3 October 2007
Available online 29 January 2008

Abstract

A three-dimensional numerical model is developed to investigate the effect of turbulence on heat and mass transfer rates of a droplet exposed to a hot airstream. The airstream turbulence, temperature and mean Reynolds number are varied to provide a wide range of test conditions. The ambient pressure is kept atmospheric. In addition, variable thermophysical properties, transient gas and liquid phases, and the effect of radiation are all considered in the numerical study. The turbulence terms in the conservation equations of the gas-phase are modelled by using the shear-stress transport (SST) model. A Cartesian grid based blocked-off technique is used in conjunction with the finite-volume method to solve numerically the governing equations of the gas and liquid phases. The numerical results indicate that the effect of freestream turbulence is persistent although it weakens as the airstream temperature increases. The effect of radiation becomes significantly important at elevated airstream temperatures. Comprehensive droplet heat and mass transfer correlations are proposed, which take into consideration all the aforementioned variables.

Keywords: Turbulence; Airstream; Numerical simulation; Droplet; Heat and mass transfer

1. Introduction

The effect of freestream turbulence on sphere (or droplet) heat and mass transfer received great attention in the past decades [1–22]. Recently, these studies are reviewed extensively by Birouk and Gökalp [23]. The conclusion of their review is that early studies prior to 1990s reported mixed conclusions. The majority of these early studies claimed an increase in sphere (or droplet) heat and mass transfer rates due to turbulence [1,3,6–22]; whereas the minority of these studies concluded that turbulence had a negligible effect on sphere heat and mass transfer, especially at low Reynolds numbers [2,4,5]. The review of Birouk and Gökalp [23] reported that all recent studies, performed after 1990s, supported the view that turbulence indeed enhances droplet heat and mass transfer. Most of these studies correlated the effect of turbulence on sphere (or droplet) heat and mass transfer in terms of Nusselt (Nu) and Sherwood (Sh) numbers, respectively, which are grouped as follows [23,24]:

$$Sh = A' + B' Re^{1/2} Sc^{1/3}(C_T) \quad (1)$$

$$Nu = A' + B' Re^{1/2} Pr^{1/3}(C_T) \quad (2)$$

where C_T is a turbulent term and, A' and B' are constants. The published turbulent Nusselt and Sherwood correlations are tabulated in Table 1 along with the corresponding values of the coefficients A', B' and C_T. Note that for droplet heat and mass transfer, Eqs. (1) and (2) are corrected by multiplying Nusselt and Sherwood numbers by $(1 + B_T)^{0.7}$ and $(1 + B_M)^{0.7}$, respectively [14,25]. *The heat and mass transfer numbers B_M and B_T are defined as* $B_T = c_{p,g}(T_\infty - T_s)/L_{evap,s}(1 - \dot{Q}_l/\dot{Q}_g + \dot{Q}_r/\dot{Q}_g)$ *and* $B_M = (Y_{F,s} - Y_{F,\infty})/(1 - Y_{F,s})$, *respectively.*

Recent studies followed different approaches to evaluate further the effect of turbulence on droplet evaporation [16–21,24,26] due to its importance for spray combustion modelling [27]. For example, Birouk et al. [18,19] and Ohta et al. [28] developed a novel approach to verify whether

* Corresponding author. Tel.: +1 204 474 8482; fax: +1 204 275 7507.
E-mail address: biroukm@cc.umanitoba.ca (M. Birouk).

0017-9310/$ - see front matter © 2007 Elsevier Ltd. All rights reserved.
doi:10.1016/j.ijheatmasstransfer.2007.12.001

Nomenclature

A	area
B_M	Spalding mass transfer number
B_T	heat transfer number
C_T	a turbulence coefficient in Eqs. (1) and (2)
c_p	constant pressure specific heat
d	droplet/sphere diameter
D_{AB}	mass diffusion coefficient
I	turbulence intensity (u'/U_∞)
K	evaporation rate
k	turbulence kinetic energy
L	latent heat of vaporization
$\dot{m}$	mass flow rate
$\dot{m}''$	mass flux
Nu	Nusselt number
Pr	Prandtl number
p	pressure
$\dot{Q}$	rate of heat transfer
$\dot{q}$	rate of heat transfer per unit area
Re	Reynolds number
r	droplet radius
$\dot{r}$	regression rate of the droplet's radius
Sc	Schmidt number
Sh	Sherwood number
S_Φ	source term ($S_\Phi = S_C + S_P\Phi$)
T	temperature
U_∞	mean freestream velocity
u	velocity component in x-direction
v	velocity component in y-direction
w	velocity component in z-direction
Y_F	fuel mass fraction

Greek symbols

μ	viscosity
σ_h	turbulent Prandtl number
λ	thermal conductivity
ω	dissipation per unit turbulence kinetic energy, ε/k
Φ	diffusion parameter (u, v, w, p, T, Y_F, k, and ω)
ρ	density
Δx	control volume length in x-direction
Δy	control volume length in y-direction
Δz	control volume length in z-direction

Subscripts

a	air
b	boiling
d	droplet
eff	effective
evap.	evaporated
f	film condition
g	gas
L	laminar
l	liquid
M	modified
m	mixture
nor	normal
s	surface
t	turbulent
tan	tangential
∞	free stream
0	initial

turbulence has really an effect on the gasification process of a droplet. They isolated the flow mean velocity from its fluctuating components and investigated only the effect of the turbulence. Their results agreed with each other and resulted in a new correlation [19] which is mainly a modification of Frössling laminar correlation [29] to account for turbulence. Gökalp et al. [16] developed a novel idea for correlating the effect of turbulence on droplet mass transfer in terms of an effective vaporization Damköhler number. The approach developed by Gökalp et al. [16] was later pursued by Hiromitsu and Kawaguchi [17] and Wu et al. [20,21]. Wu et al. [21] employed a wide range for turbulent flow and liquid properties and established a correlation in terms of a vaporization Damköhler number, which is expressed as follows: $K/K_L = 0.771Da_v^{-0.111}$, where K and K_L are the droplet evaporation rates under turbulent and laminar flow conditions, respectively. Da_v is the vaporization Damköhler number, which is defined as the ratio of a turbulence characteristic time t_t over an evaporation characteristic time t_v ($Da_v = t_t/t_v$), where $t_t = (d_0)^{2/3}/\varepsilon^{1/3}$ and $t_v = \delta_M/V_r$. δ_M and V_r are the vapour film thickness around the droplet and vapour blowing velocity, respectively [20,23]. Hiromitsu and Kawaguchi [17] claimed that the concept of a correlation in terms of a vaporization Damköhler number would not work at elevated temperatures. Recently, Abou Al-Sood [30], and Abou Al-Sood and Birouk [24] developed a numerical study to take part of the aforementioned debate. It was found that the Damköhler number in its current form could indeed correlate the droplet turbulent evaporation rate but only at standard airstream temperature conditions. Abou Al-Sood and Birouk [24] adopted Eq. (1) to develop a correlation which accounts for the effect of freestream turbulence on droplet mass transfer. This correlation, which has a similar form to Eq. (1), is expressed as follows [24,30]:

$$Sh_f(1 + B_{M,f})^{0.7} = 2 + 0.914Re_M^{1/2}Sc_f^{1/3}(1 + 1.235I_\infty^{0.372}) \quad (3)$$

where B_M, Re, Sc and I are the mass transfer number, Reynolds number, Schmidt number and turbulence intensity, respectively. The subscripts f and ∞ denote film and free stream conditions. Although this correlation worked well

Table 1
Summary of published sphere (or droplet) heat and mass transfer correlations

Reference	Nu or Sh	A'	B'	C_T	Validity
Galloway and Sage [7]	Nu or Sh	2	1.0	$0.562 + 0.1807d^{1/2} + 0.0672I_\infty \times (I_\infty + 0.05)Re_\infty^{1/2}$	$0.01 \leqslant I_\infty \leqslant 0.15$ $2 \leqslant Re_\infty \leqslant 1.33 \times 10^6$ $0.02'' \text{ in} \leqslant d \leqslant 12''$
Galloway and Sage [7]	Nu	2	1.0	$0.538 + 0.1807d^{1/2} + 0.328I_\infty(I_\infty + 0.0405)Re_\infty^{1/2}$	$0.01 \leqslant I_\infty \leqslant 0.15$ $2 \leqslant Re_\infty \leqslant 1.33 \times 10^6$
Galloway and Sage [7]	Sh	2	1.0	$0.439 + 0.1807d^{1/2} + 0.234I_\infty(I_\infty + 0.0500)Re_\infty^{1/2}$	$0.01 \leqslant I_\infty \leqslant 0.15$ $2 \leqslant Re_\infty \leqslant 1.33 \times 10^6$
Lavender and Pei [9]	Nu	2	0.717	$(ReI_\infty)^{0.035}$	$ReI_\infty < 1000$
	Nu	2	0.165	$(ReI_\infty)^{0.250}$	$ReI_\infty > 1000$
Yuge [4] correlated by Lavender and Pei [9]	Nu	2	0.387	$(ReI_\infty)^{0.085}$	$ReI_\infty < 7000$
Gostkowski and Costello [11]	Nu	0	1.431	$(ReI_\infty)^{0.0214}$	$ReI_\infty < 7000$
	Nu	0	1.287	$(ReI_\infty)^{0.2838}$	$ReI_\infty > 7000$
Sandoval-Robles [13]	Sh	0	0.549	$(ReI_\infty)^{0.066}$	$12 < ReI_\infty < 600$
Yearling [14]	$Nu(1 + B_T)^{0.7}$	2	0.58	$1 + 3.397I_\infty^{0.843}$	$0.01 \leqslant I_\infty \leqslant 0.11$
	$Sh(1 + B_M)^{0.7}$	2	0.52	$1 + 3.397I_\infty^{0.843}$	$50 < Re < 1500$
Refai-Ahmed *et al.* [15]	Nu	0	0.465	$Re^{0.109}I_\infty^{0.174}$	$0.012 \leqslant I_\infty \leqslant 0.049$ $5.6 \times 10^4 < Re < 5.6 \times 10^4$
Abou Al-Sood and Birouk [24]	$Sh(1 + B_M)^{0.7}$	2	0.914	$1 + 1.235I_\infty^{0.372}$	$0.01 \leqslant I_\infty \leqslant 0.6$ $17 < Re < 186$
Present study	$Nu(1 + B_T)^{0.7}$	2	0.677	$1 + 0.455I_\infty^{0.372}$	$0.01 \leqslant I_\infty \leqslant 0.6$ $17 < Re < 186$

for a wide range of turbulent flow and liquid fuel properties, the effect of radiation which can be important was neglected. Therefore, the aim of the present study is to verify/extend the applicability of this mass transfer correlation by taking into consideration the effect of radiation. It is also the aim of the present study to propose a droplet heat transfer correlation in terms of Nusselt number based on Eq. (2).

2. Mathematical model

2.1. Description of the physical model and assumptions

Consider a hydrocarbon fuel droplet, with an initial radius of r_0 and an initial uniform temperature T_0, immersed in a turbulent inert airstream of infinite expanse. The gas-phase is prescribed by its freestream mean velocity, U_∞, pressure, p_∞, temperature, T_∞, fuel mass fraction, $Y_{F\infty}$, turbulence intensity, I_∞, and turbulence kinetic energy, k_∞, and its dissipation per unit of turbulence kinetic energy, ω_∞. The droplet and its surrounding conditions are schematically shown in Fig. 1.

The following assumptions are employed in the present model: (i) the droplet is stationary and consists of a single chemical component, (ii) the droplet shape remains spherical because the droplet Weber number is much less than unity, (iii) the droplet evaporates in an inert atmosphere, (iv) the gas–liquid interface is at an equilibrium phase, (v) Dufour (energy flux due to mass concentration) and Soret effects (mass diffusion due to temperature) are assumed negligible, and (iv) radiation is considered with the assumption that the gas-phase between the droplet and the wall is transparent and does not emit any radiation, and the wall, which is chosen here as the boundary of the calculation domain, is assumed as blackbody emitter with a temperature equals to that of the freestream.

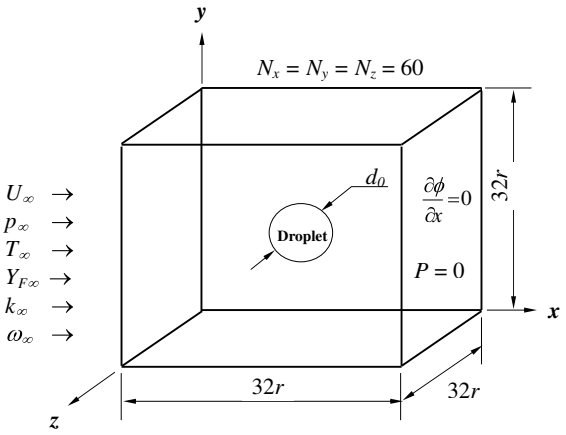

Fig. 1. Schematic of the physical problem along with the initial and boundary conditions of a droplet exposed to a turbulent freestream.

2.2. Governing equations

The governing equations for the gas-phase are the Reynolds-Averaged Navier–Stokes (RANS), energy and mass species conservation equations. Details of these equations with the adopted turbulence closure model, i.e. shear-stress transport (SST) model of Menter [31], are reported in previous publications [24,26,30,32]. For the liquid phase (i.e. droplet), the governing equations are basically the unsteady continuity, momentum and energy equations, which are given as

$$\frac{\partial \rho}{\partial t} + \frac{\partial}{\partial x_i}(\rho u_i) = 0 \tag{4}$$

$$\frac{\partial}{\partial t}(\rho u_i) + \frac{\partial}{\partial x_j}(\rho u_i u_j) = -\frac{\partial p}{\partial x_i} + \frac{\partial}{\partial x_j}\left(\mu \frac{\partial u}{\partial x_j}\right) \tag{5}$$

$$\frac{\partial}{\partial t}(\rho c_p T) + \frac{\partial}{\partial x_j}(\rho u_i c_p T) = \frac{\partial}{\partial x_j}\left(\frac{\mu c_p}{Pr}\frac{\partial T}{\partial x_j} - \dot{q}_r\right) \tag{6}$$

where $\dot{q}_r$ is the radiative absorption rate per unit area.

2.3. Radiative heat transfer model

The radiation field inside a homogeneous liquid fuel droplet can be modeled by either of the two following methods; (i) the radiative transfer theory (geometrical optics) [33,34], or (ii) the electromagnetic waves theory [35]. While, the latter neglects the radiation losses, the former is not applicable for small droplet. For large droplet, the radiation absorption by the liquid phase is limited to a thin subsurface layer [33]. Since the study of radiation is beyond the scope of the present investigation and the droplet is large enough, an approximation of the radiation absorption that occurs only at the droplet surface with an effective surface absorptance α_{eff} (as $\dot{q}_r = \alpha_{\text{eff}}\sigma(T_\infty^4 - T_s^4)$) is considered in this study for the sake of simplicity. The value of the effective surface absorptance is based on the data of Tseng and Viskanta [34], which is a function of the droplet diameter and ambient temperature. In the present study, the value of α_{eff} for *n*-decane, which is not readily available in the open literature, is assumed approximately equal to that of diesel fuel.

2.4. Freestream and gas–liquid interface conditions

The freestream mean velocity components, pressure, temperature, fuel mass fraction and turbulence quantities at the inlet of the computational domain are taken as $u = U_\infty$, $v = 0$, $w = 0$, $p = p_\infty$, $T = T_\infty$, $Y_F = 0$, $k = k_\infty$ and $\omega = \omega_\infty$. The freestream k_∞ and ω_∞ are estimated by using the following relations as [31,36] $k_\infty = 1.5(I_\infty \times U_\infty)^2$ and $\omega_\infty = \rho_\infty(k_\infty/\mu_\infty)(\mu_{t\infty}/\mu_\infty)^{-1}$ where $\mu_{t\infty}$ is the freestream turbulent viscosity which is taken as $\mu_{t\infty} \cong (0.1 - 10)\mu_\infty$. A distinctive gas–liquid interface exists at the droplet surface and conditions at this interface are obtained by coupling the conservation equations (momentum, energy and species equations) in the gas and the liquid phases as follows [30]:

(a) Shear-stress continuity

$$\tau_{ij,g} = \tau_{ij,l} \tag{7}$$

(b) Tangential velocity continuity

$$U_{\tan}|_g = U_{\tan}|_l = U_s \tag{8}$$

(c) Normal velocity continuity

$$U_{\text{nor}}|_l = \left(\frac{\rho_g}{\rho_l}\right)U_{\text{nor}}|_g + \dot{r}\left(1 - \frac{\rho_g}{\rho_l}\right) \tag{9}$$

(d) Temperature continuity

$$T_g = T_l = T_s \tag{10}$$

(e) Energy conservation

$$\lambda\frac{\partial T}{\partial x_i}\bigg|_l = \lambda_{\text{eff}}\frac{\partial T}{\partial x_i}\bigg|_g - \dot{m}''_{\text{evap}}h_{\text{evap}} + \dot{q}_r \tag{11}$$

(f) Species conservation

$$\dot{m}''_{\text{evap}}(Y_{F,g} - 1) - \rho_g D_{AB,g}\frac{\partial Y_{F,g}}{\partial x_i} = 0 \tag{12}$$

(g) Droplet mass conservation

$$\dot{r} = -\frac{\sum_{\text{evaporated surfaces}}\dot{m}''_{\text{evap},i}A_s}{4\pi\rho r^2} + \frac{r}{3\rho}\frac{d\rho}{dt} \tag{13}$$

where the subscripts g and l denote any variable in the gas and liquid sides at the droplet-gas interface, respectively. The parameter $\dot{r}$ denotes the regression rate of the droplet radius, r is the instantaneous droplet radius, and A_s is the surface area of the nodes subjected to the flow. The last term in Eq. (13) is due to the swelling of the droplet during its warming-up period. The effect of turbulence on droplet heat and mass transfer processes is accounted for in the energy and species equations (Eqs. (11) and (12)) via the effective thermal diffusivity, λ_{eff}, and the effective molecular mass diffusion, $D_{AB,g}$, respectively. These two parameters are defined as [30] $\lambda_{\text{eff}} = (\mu/\text{Pr}) + (\mu_t/\sigma_h)$ and $D_{AB,g} = D_{AB} + (\mu_t/Sc_t)$. Note that in the case of laminar flow, both turbulent terms (second term from the right hand side) cancel out.

3. Numerical approach

To solve the complex nonlinear and strongly coupled set of governing transport equations, a finite-volume approach [37] was employed. The governing differential equations were integrated over discrete volumes resulting in a set of algebraic equations having the following general form

$$\begin{aligned}(a_E + a_W + a_N + a_S + a_T\Phi_T + a_B - S_P\Delta x\Delta y\Delta z)\Phi_P \\ = a_E\Phi_E + a_W\Phi_W + a_N\Phi_N + a_S\Phi_S + a_T\Phi_T + a_B\phi_B \\ + S_C\Delta x\Delta y\Delta z\end{aligned} \tag{14}$$

where a_P, a_E, a_W, a_N, a_S, a_T, a_B, and b_Φ are coefficients and their expressions are reported in [26,30]. S_P and S_C are the two terms of the linearized source term S_Φ. Δx, Δy, and Δz are the control volume lengths in the direction of x, y, and z coordinates, respectively. The absence of an explicit equation for pressure is dealt with by using the SIMPLEC approach [38] in which an expression in the form of Eq. (14) is derived for the pressure through a combination of the continuity and momentum equations. The aim is to develop a pressure field such that the resulting velocity field satisfies the continuity equation for every control volume in the calculation domain.

The spherical liquid droplet in the Cartesian grid is treated by using a blocking-off technique. Details about the block-off technique can be found in [24,26,30,32]. The calculation domain, which is a cube of $32r \times 32r \times 32r$, where r is the droplet radius, is divided into several control volumes and the droplet is fixed at the center of the cube [24]. Fig. 1 summarizes the computational domain and boundary conditions where the left and right faces are inflow and outflow boundary conditions, respectively, whereas the remaining faces are taken as the wall boundary conditions. In the present analysis, the Cartesian grid in the calculation domain consists of $60 \times 60 \times 60$. Since the gradients around the sphere are large, a very fine grid, $40 \times 40 \times 40$ is used in the domain of $4r$, i.e., $2r$ from the droplet center in all directions. This number of grids is found to be the optimum number that provides stable results with an acceptable computational time. More information about the sensitivity of the results to the chosen grid is reported in [30].

The solution of the set of linearized algebraic equations is accomplished by using three-dimensional vectorized version of SIP (Strongly Implicit Procedure) developed by Leister and Peric [39]. The iterative solution of the governing equations is performed for each time step until one of the two imposed conditions is achieved, i.e. either the assigned maximum number of iterations is exceeded or the range-normalized relative errors of the diffusion parameter (u, v, w, p, T, Y_F, k, and ω) expressed as $|(\Phi^{n+1} - \Phi^n)/(\Phi_{max} - \Phi_{min})| \leqslant \varepsilon_\Phi$ are satisfied for each node. Note that Φ_{max} and Φ_{min} are the maximum and minimum values for the entire Φ^{n+1} field and ε_Φ is taken equal 10^{-4} for all quantities. The calculations are terminated when the droplet diameter is less than 1/10 of its initial value (i.e. $d < 0.1d_0$), where d and d_0 are the droplet instantaneous and initial diameters, respectively.

4. Results and discussion

The test conditions are given in Table 2 and the formula employed to calculate the thermodynamic properties of *n*-heptane and *n*-decane droplets, as well as those of the vapour–air mixture in the droplet surface vicinity are reported in previous publications of the present authors [24,30].

4.1. Validation of the numerical model

The numerical model developed in the present study is verified by comparing its predictions with their published numerical and experimental counterparts. Fig. 2 exhibits a comparison of the evaporation rate of *n*-heptane and *n*-decane droplets between the present predictions and published experimental data. Note that the numerical data shown in Fig. 2 are similar to those presented in Ref. [26] except that the effect of radiation is considered in the present predictions, but it is neglected in Ref. [26]. Nevertheless, the effect of radiation is appeared negligible at standard room temperature where only an increase of 0.5% and 0.1% in the evaporation rate of *n*-heptane and *n*-decane, respectively, is noticed due to radiation. The present numerical model has been validated for predicting the droplet turbulent vaporization under standard pressure and temperature conditions [26]. Fig. 2 demonstrates clearly that the predictions are in excellent agreement with published experimental data. Published data for droplet evaporation in turbulent flow at elevated ambient temperatures are not available. Thus, validation of the present numerical model is performed by comparing the present predictions with their counterparts published numerical and experimental published data under only laminar flow conditions. Fig. 3 presents the time-history of the squared normalized diameter of *n*-decane droplet as predicted by the present numerical model. The same figure shows a comparison of the present predictions against the laminar numerical data of Abou Al-Sood and Birouk [24] and Megaridis [40], and the laminar experimental data of Wong and Lin [41]. The data presented in Fig. 3 are obtained for a Reynolds number of 17 and a typical freestream temperature $T_\infty = 1000$ K. Fig. 3 exhibits two major distinct

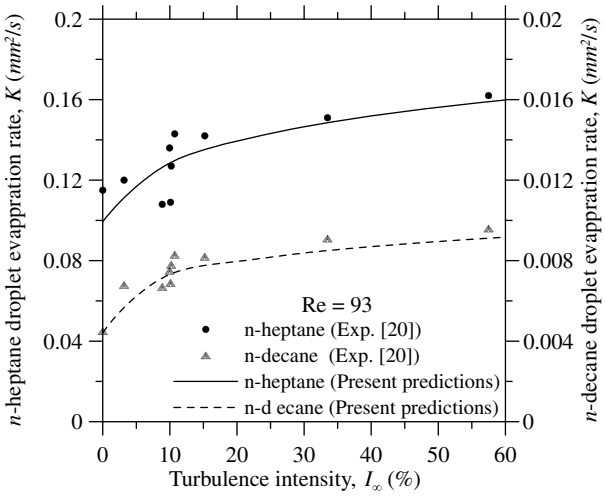

Fig. 2. Variation of the evaporation rates of *n*-heptane and *n*-decane droplets versus freestream turbulence intensity.

Table 2
Test conditions

	d_0 (mm)	U_∞ (m/s)	I_∞ (%)	P_∞ (atm)	T_∞ (K)	Re_∞
Stagnant	0.7	0	0	1	474, 555, 741	
Laminar	1.96, 1.50	0.6, 1, 2	0	1	300–1273	17–186
Turbulent	1.50	0.6, 2	5–60	1	300–1273	17–186

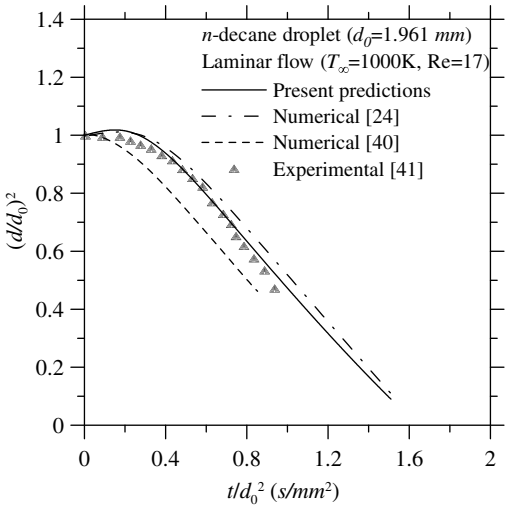

Fig. 3. Time-history of the normalized squared diameter of *n*-decane droplet as predicted by the present model and compared with published experimental and numerical data (the droplet initial temperature, $T_{d,0}$, is 320 K in the present study as well as in Refs. [24,40]).

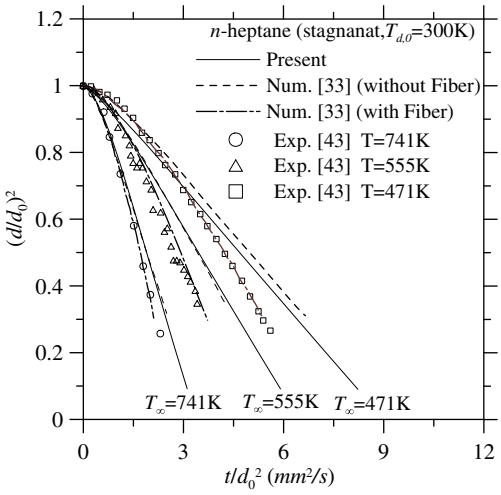

Fig. 4. Time-history of *n*-heptane droplet squared diameter in stagnant flow at various ambient temperatures (both present, and Yang and Wang [33], numerical predictions are obtained with the effect of radiation included).

zones. The first one concerns the transient phase (i.e., the heating-up period) of the droplet. During this phase, the present predictions exhibit reasonably comparable droplet's swelling and heating period compared to those observed in [41]. The slight difference is attributed to the effect of the droplet support/fiber used in the experiment [41], which enhances the droplet heat transfer by conduction. However, no droplet' swelling is present in the predictions of Ref. [40] and also the droplet heating period is much shorter compared to the present predictions. This noticeable difference is due mostly to the assumption of constant droplet density, and to some extent the effect of radiation which is neglected in Ref. [40]. Recall that the effect of radiation is more pronounced during this phase, as the droplet is at its largest volume (i.e. largest surface area as the liquid density varies with temperature) where the effective absorptance is directly proportional to the droplet diameter [34,42]. The second remarkable zone of the evolution of $(d/d_0)^2$ concerns the droplet steady-state evaporation phase. It appears in Fig. 3 that during this phase, the linear variation of $(d/d_0)^2$ versus the normalized droplet evaporation time (i.e. the droplet evaporation rate) is identical for all numerical studies (i.e. [24,40]) including the present predictions. However, the slop of the experiment of Ref. [41] deviates slightly from the numerical predictions which is due to the effect of the droplet supporting material as discussed below in Fig. 4. It is clear thus that overall the present numerical predictions with the effect of radiation considered are in much better agreement with the experimental data throughout the droplet life-time. To evaluate further the radiation model adopted in the present study, a comparison of the variation of *n*-heptane droplet lifetime between the present predictions and their published counterparts is plotted in Fig. 4 for various ambient temperatures. The corresponding droplet evaporation rates are tabulated in Table 3. The plots in Fig. 4 and the data presented in Table 3 show that the radiation model adopted in the present study produces approximately similar results to the numerical data of Yang and Wang [33]. However, both studies (i.e. the present study and that in Ref. [33]) predict lower droplet vaporization rate (i.e. longer droplet lifetime) when compared with their experimental counterparts [43]. The discrepancy between the numerical predictions and experimental data, shown in Fig. 4, is attributed to the effect of the fiber onto which the droplet is suspended, which is found to enhance significantly the droplet heat transfer and hence mass transfer [33]. In addition, a comparison of the instantaneous droplet surface temperature between the present predictions and those of Sazhin et al. [44] are plotted in Fig. 5 for several ambient temperatures. This figure shows that the droplet surface temperature increases until it reaches a maximum value, which is higher than the wet bulb temperatures, after which it decreases towards the droplet wet bulb temperature. This trend in the variation of the droplet surface temperature, which is related to the effect of thermal radiation, is discussed in Ref. [42]. The difference between both predictions, which is less than 3%, is due to the difference in the value of the effective surface absorptance, α_{eff},

Table 3
n-Heptane droplet evaporation rate calculated from Fig. 4 (the percent error in this table is calculated with respect to the experimental data of Nomura et al. [43]).

Evaporation rate, K (mm^2/s)			
T_∞ (K)	Present data	Yang and Wang [33]	Nomura et al. [43]
471	0.1161 (27.2%)	0.1163 (27.1%)	0.1595
555	0.1672 (25.9%)	0.1753 (22.3%)	0.2255
741	0.3384 (15.9%)	0.3122 (22.4%)	0.4024

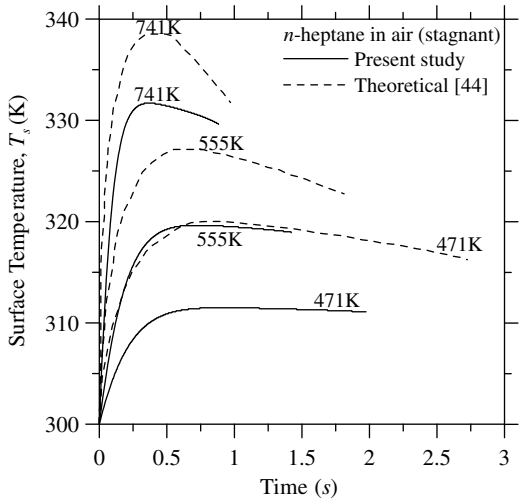

Fig. 5. Time-history of *n*-heptane droplet surface temperature for various ambient temperatures.

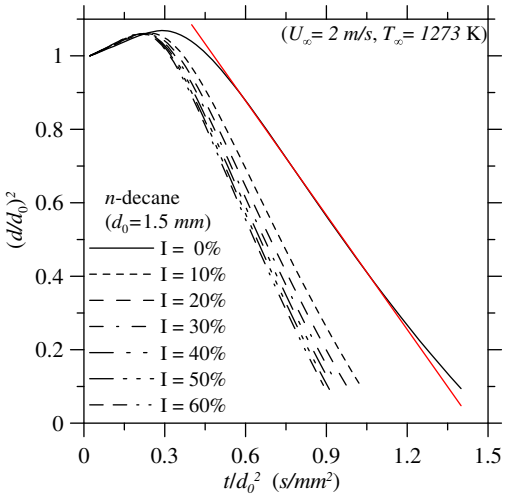

Fig. 7. Time-history of the normalized squared diameter of *n*-decane droplet at $T_\infty = 1273$ K and $U_\infty = 2$ m/s for various freestream turbulence intensities ($d_0 = 1.5$ mm and $T_{d,0} = 253$ K).

employed in both studies. In the present study the value of α_{eff} is in the range between 0.40 and 0.60 depending on T_∞ as suggested in Ref. [34], whereas it is constant, 0.93, in Ref. [44].

4.2. Turbulence effect on droplet heat and mass transfer

Figs. 6 and 7 show the time-history of the normalized squared diameter of *n*-heptane and *n*-decane droplet, respectively, for a typical freestream mean velocity of 2 m/s, a wide range of freestream turbulence intensity and a freestream temperature of 1273 K. For both fuel types, these figures show that the droplet heating period becomes shorter as the freestream turbulence intensity increases. In addition, the droplet lifetime decreases with increasing turbulence intensity. Furthermore, it is interesting to note that the freestream turbulence still has an effect

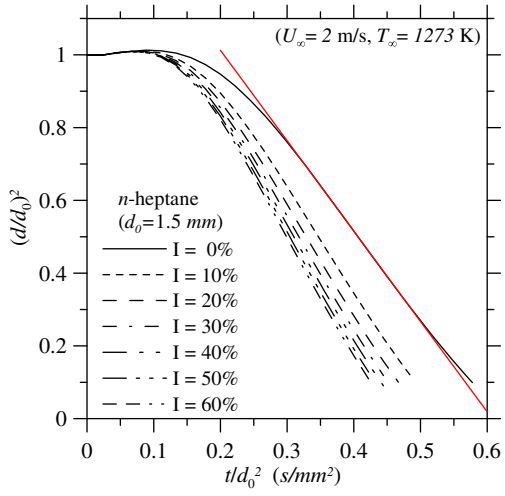

Fig. 6. Time-history of the normalized squared diameter of *n*-heptane droplet at $T_\infty = 1273$ K and $U_\infty = 2$ m/s for various freestream turbulence intensities ($d_0 = 1.5$ mm and $T_{d,0} = 253$ K).

on the droplet's evaporation rate even at elevated freestream temperatures. More interestingly, Figs. 6 and 7 demonstrate that the d^2-law holds during the majority of the droplet evaporation phase (which is preceded by the heating period). However, the d^2-law departs during the very end portion of the droplet lifetime. For example, it occurs after about 70% of the *n*-decane droplet mass is evaporated (i.e. in the region where $d < 0.3d_0$). The non-linearity of this portion of the d^2, in which the droplet evaporation slows down, is mainly caused by a decrease in the heat transfer by radiation as a result of a decrease in the droplet surface area. It is important to mention that according to the present predictions, the d^2-law departure occurs only at ambient temperatures exceeding approximately 800 K. The observation that d^2-law holds at elevated ambient temperatures appears to contradict that of Sazhin et al. [44] who claim that the d^2-law does not hold for ambient temperatures $T_\infty > 700$ K when considering the effect of radiation. Conversely, the present predictions with the effect of radiation considered are in agreement with those of Yang and Wong [33] who showed numerically that the d^2-law holds at similar ambient gas temperatures. Recall that the effect of thermal radiation is also considered by Yang and Wong [33]. The discrepancy between the present predictions and those of Yang and Wong [33] with the predictions of Sazhin et al. [44] might be caused by the variation of the droplet surface temperature. As shown in Fig. 5, Sazhin et al. [44] predict that the droplet surface temperature decreases sharply after reaching a maximum value, whereas in the present study, the droplet surface temperature decreases almost unnoticeably.

Fig. 8 presents the time-history of the surface temperatures of *n*-heptane and *n*-decane droplets for different turbulence intensities at typical values of the ambient temperature and freestream mean velocity. This figure shows that for a given fuel type, the droplet surface temperature

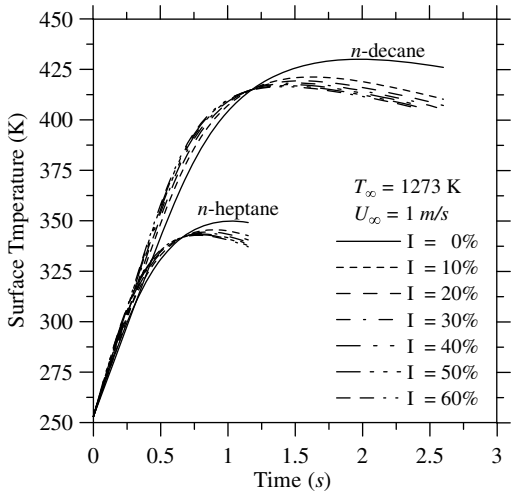

Fig. 8. Time-history of *n*-heptane and *n*-decane droplets surface temperature for different airstream turbulence intensities.

increases until it reaches a maximum value higher than the corresponding wet bulb temperature which is then followed by a slight decrease towards the wet-bulb value. This trend of the droplet surface temperature is related to the effect of thermal radiation as discussed in Abramzon and Sazhin [42]. Fig. 8 reveals also another interesting observation in which an increase in turbulence intensity decreases the maximum droplet surface temperature. This might be due to the increase in the heat transfer from the gas-phase by convection, q''_g, which accelerates the droplet evaporation. Note that a decrease in the droplet's diameter leads to a less heat transfer by radiation, as $q''_r \propto d^{2.5}$ [42]. Lifetime of *n*-heptane and *n*-decane droplets as a function of freestream turbulence intensity for various freestream temperatures is presented in Fig. 9. Several distinct observations can be noticed in Fig. 9. The effect of radiation is more pronounced for the least volatile fuel (i.e., *n*-decane). This is because the droplet evaporation rate, which corresponds to a decrease in the droplet diameter, is much slower for the least volatile fuel (i.e. *n*-decane). Also, the effect of radiation is higher for weak turbulence intensities. For instance, *n*-heptane droplet lifetime at 1273 K is reduced (as compared to that with neglected radiation) by 27% and 23.1% for turbulence intensities of 0% and 60%, respectively. These observations can be explained as follows. The droplet evaporation rate, which engenders a decrease in the droplet diameter, is much slower for weak turbulence, and hence the heat transfer by radiation is relatively higher under these conditions ($q''_r \propto d^{2.5}$) as d decreases slowly. Another observation in Fig. 9 is that the droplet lifetime is much shortened as the freestream turbulence increases. For example, the *n*-decane droplet lifetime is reduced due to an increase of freestream turbulence from 0% to 60% by 53.3%, 41.8%, and 36.5% at 300 K, 773 K and 1273 K, respectively. In addition, Fig. 9 indicates that the effect of radiation is nearly negligible for temperature less than around 773 K, where its effect is found less than 6% regardless of the fuel type. Fig. 10 illustrates the variation of the *n*-heptane and *n*-decane

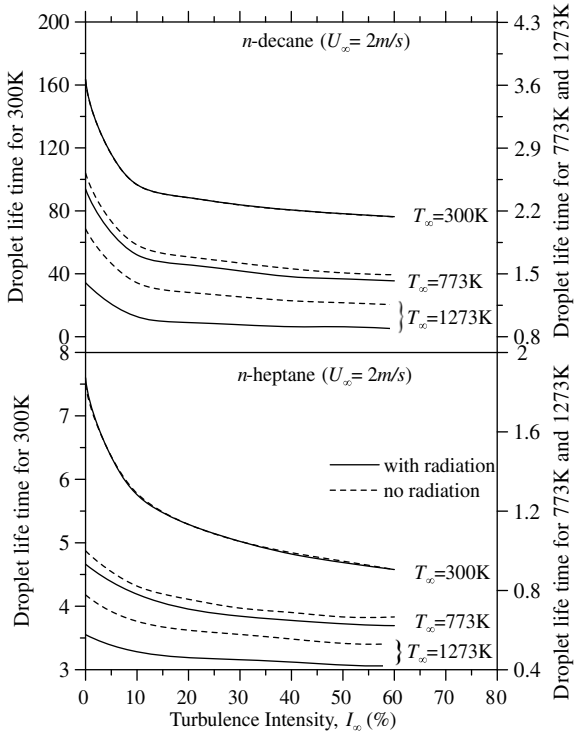

Fig. 9. Droplet life-time versus the freestream turbulence intensity at a mean velocity $U_\infty = 2$ m/s, and various freestream temperatures.

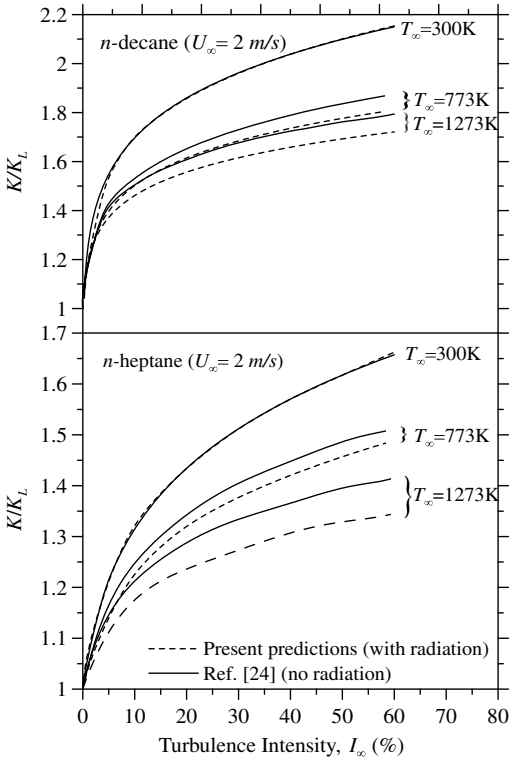

Fig. 10. K/K_L of *n*-heptane and *n*-decane droplets versus turbulence intensity at a typical mean velocity $U_\infty = 2$ m/s and various temperatures.

droplets' turbulent evaporation rates normalized by their corresponding laminar values, K/K_L, for three typical ambient temperatures, i.e. 300 K, 773 K and 1273 K. The solid and dashed lines presented in Fig. 10 are calculated, respectively, by neglecting and taking into consideration the effect of radiation. Fig. 10 demonstrates that the effect of turbulence is much more pronounced at low to moderate turbulence intensities (i.e. $I_\infty \sim <20$). The same figure shows that the effect of radiation becomes significant as the ambient temperature increases, and hence cannot be neglected.

Fig. 11 presents a comparison of the turbulent mass transfer correlation which is proposed previously [24,30] with the present predictions, which are obtained under similar test conditions but with the effect of radiation is considered in the present calculations. This figure shows that there is a slight deviation of less than 5%, which occurs especially at relatively lower Reynolds numbers (i.e. at relatively high temperatures). As the droplet mass transfer is very much coupled with droplet heat transfer, it is also important to develop a correlation for droplet heat transfer, which is also essential for modeling more complex spray flows. Thus, the data presented above are employed to develop a correlation for heat transfer of a droplet evaporating in a turbulent hot airstream. The test conditions, which are employed here, are the same as for the droplet mass transfer correlation presented in Fig. 11, which are summarized in Table 2. The conventional form of droplet heat transfer correlation, that is Eq. (2), is adopted. Note that the Nusselt number is calculated as discussed in Appendix A. Since the droplet surface temperature does not approach a constant value at higher freestram temperatures due to radiation (as shown in Figs. 5 and 8), the Nusselt number of the droplet steady-state evaporation phase is calculated as the average value of the temporal Nusselt number which corresponds to the steady-state region where the d^2-law holds, as shown in Figs. 6 and 7.

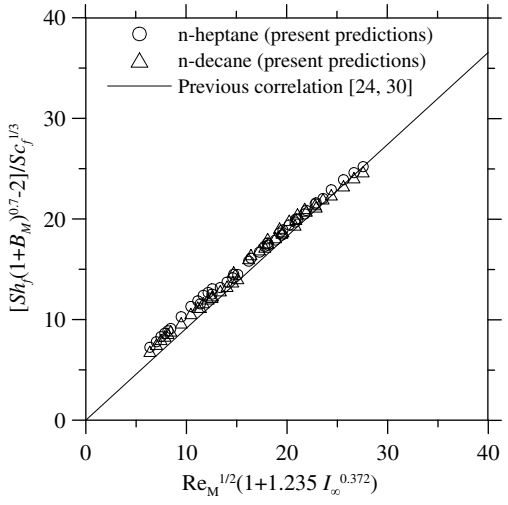

Fig. 11. Comparison of the predicted Sherwood number for *n*-heptane and *n*-decane droplets with the correlation proposed in [24,30].

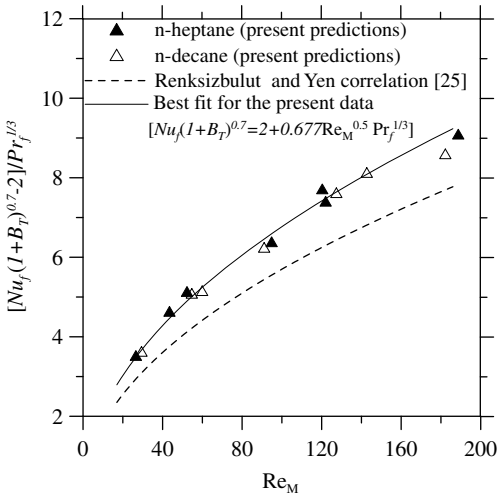

Fig. 12. Laminar Sherwood number for *n*-heptane and *n*-decane droplets versus Reynolds number for flow temperature ranging between 300 K and 1273 K.

Fig. 12 presents the variation of the steady-state average Nusselt number versus Reynolds number. This figure shows that although the predicted steady-state laminar Nusselt number has exactly similar trend to that of Renksizbulut and Yuen [25], the present predictions manifest slightly higher values. It is important to mention that the same radiation model is employed in [25] and in the present numerical study ($\dot{q}_r = \alpha_{eff}\sigma(T_\infty^4 - T_s^4)$). The difference is that a constant value for effective surface absorptance (i.e. $\alpha_{eff} = 0.95$) for all droplets and flow conditions is employed in Ref. [25]; whereas it is varied in the present investigation (i.e. $0.42 < \alpha_{eff} < 0.89$) as its value depends very much on the droplet and flow conditions [34]. Therefore, the higher value of α_{eff} which is used by Renksizbulut and Yen [25] yields higher radiative heat transfer, and consequently lower convective heat transfer which results in a lower Nusselt number (see Eqs. (A1) and (A2), assuming both the other two terms in Eq. (A2) vary similarly in both studies, i.e. the present and Ref. [25]). Another possible contributing factor to the discrepancy shown in Fig. 12 could be due to the reference conditions for calculating the thermodynamics properties; where 1/3 and 1/2 rules are, respectively, employed in the present study and Renksizbulut and Yen [25]. The variation of the predicted steady-state Nusselt number versus Reynolds number for different freestream turbulence intensities and ambient temperatures, which range between 0% and 60% and, from 300 K to 1273 K, respectively, are presented in Fig. 13. Reynolds numbers are calculated based on three mean velocities, i.e. 0.6 m/s, 1m/s and 2 m/s. Fig. 13 shows that for the same Reynolds number, Nusselt number increases with increasing freestream turbulence intensity. The conventional form of droplet heat transfer, i.e. Eq. (2), is found applicable to correlate the variation of the droplet steady-state Nusselt number versus the freestream turbulence intensity. The best fit for the present predicted data is

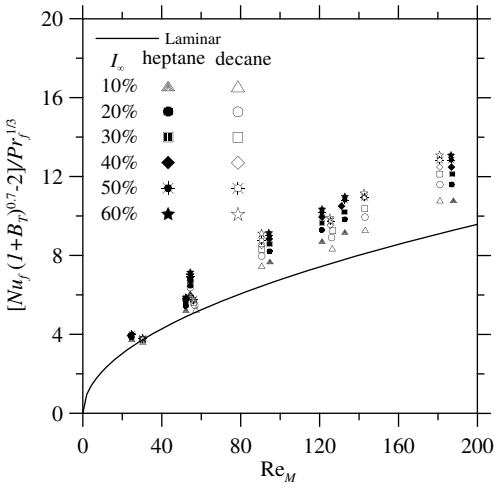

Fig. 13. Variation of Nusselt number for *n*-heptane and *n*-decane droplets with Re_M for different turbulence intensities.

found to have the following expression (with a standard deviation of 99.5%).

$$Nu_f(1+B_T)^{0.7} = 2 + 0.677Re_M^{1/2}Pr_f^{1/3}(1+0.455I_\infty^{0.372}) \quad (15)$$

This correlation, which is displayed in Fig. 14, contains the predicted data for *n*-heptane and *n*-decane droplets at ambient temperatures in the range between 300 K and 1273 K, freestream mean velocity of 0.6 m/s, 1 m/s and 2 m/s, and turbulence intensity ranging between 0% and 60%. The proposed correlation (Eq. (15)) is compared with previously published data as shown in Fig. 15. This Figure indicates that the present predictions show a reasonable agreement with the correlation of Galloway and Sage [7], as well as with the experimental data of Yearling [14], although Yearling's data are quite scatted around the proposed correlation, and Galloway and Sage's correlation deviates slightly at high turbulent coefficient, C_T.

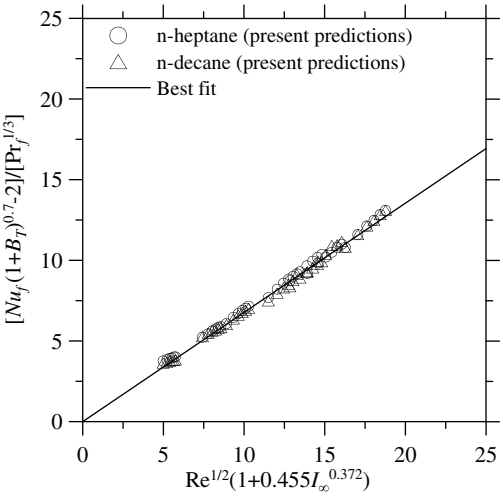

Fig. 14. Predicted turbulent Nusselt numbers for *n*-heptane and *n*-decane versus Reynolds number.

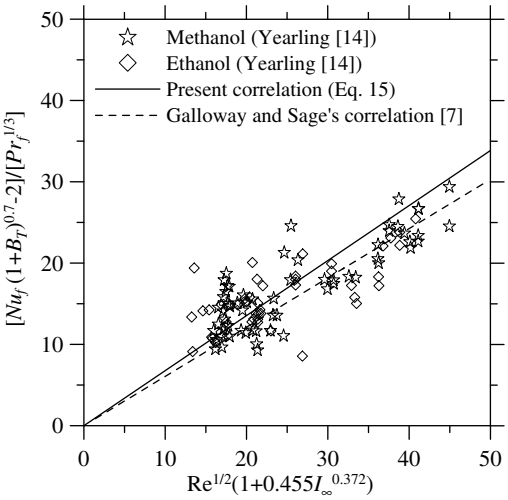

Fig. 15. Comparison of the present Nusselt number correlation with published data.

5. Conclusions

A three-dimensional numerical model is developed to assess the effect of freestream turbulence intensity on heat and mass transfer of a droplet exposed to a turbulent, hot airstream. The ambient flow conditions and liquid properties are varied to provide a wide range of test conditions. The major findings of the present study are as follows. The effect of freestream turbulence on droplet evaporation is apparent even at very high ambient temperatures, although it weakens when compared to low and moderate turbulence intensity levels. In addition, the effect of radiation which is negligible at relatively low ambient temperatures becomes significant as the freestream temperature approaches approximately 1000 °C. Also, radiation is more pronounced for the less volatile fuel. The effect of radiation on the previously proposed droplet mass transfer correlation is assessed and found that radiation causes a slight deviation (i.e. less that 5%), which occurs especially at low Reynolds numbers (i.e. at relatively high-temperatures). Finally, the effect of turbulence on droplet heat transfer is correlated in terms of Nusselt number. A comparison of the present droplet heat transfer correlation shows a satisfactory agreement with published data.

Acknowledgement

The financial support for this research is provided by the Natural Sciences and Engineering Research council of Canada (NSERC).

Appendix A

Sherwood number is calculated by the same method mentioned in [25,24,30]. Nusselt number is calculated by using the gas-phase convective heat transfer rate $\dot{Q}_g$, droplet diameter *d*, mixture thermal conductivity, freestream

temperature T_∞, and droplet surface temperatures T_s as follows:

$$Nu = \dot{Q}_g/[\pi d\lambda_f(T_\infty - T_s)] \quad (A1)$$

where the convective heat transfer rate is calculated as

$$\dot{Q}_g = \dot{m}_{evap}L_{evap} + \dot{Q}_l - \dot{Q}_r \quad (A2)$$

where L_{evap} is the latent heat of evaporation at surface temperature, and it is calculated by Watson equation $L_{evap,s} = L_{evap,b}[(T_c - T_s)/(T_c - T_b)]^{0.38}$. B_T is the modified heat transfer number and is defined as $B_T = c_{p,g}(T_\infty - Y_s)/L_{evap,s}(1 - \dot{Q}_l/\dot{Q}_g + \dot{Q}_r/\dot{Q}_g)$. All mixture's properties are calculated at reference conditions of temperature and fuel mass fraction which are expressed as

$$T_f = T_s + (T_\infty - T_s)/3 \quad (A3)$$

$$(Y_{F,s})_f = Y_{F,s} + (Y_{F,\infty} - Y_{F,s})/3 \quad (A4)$$

Prandtl and Reynolds numbers of gas mixture are calculated as $Pr_f = \mu_f c_{p,f}/\lambda_f$, and $Re_m = \rho_\infty d U_\infty/\mu_f$, respectively.

References

[1] D.S. Maisel, T.K. Sherwood, Effect of air turbulence on rate of evaporation of water, Chem. Eng. Prog. 46 (4) (1950) 172–175.

[2] N.T. Hsu, B.H. Sage, Thermal and material transfer in turbulent gas stream: local transport from spheres, AIChE J. 3 (3) (1957) 405–410.

[3] R.A.S. Brown, K. Sato, B.H. Sage, Material transfer in turbulent gas stream. Effect of turbulence on macroscopic transport from spheres, Chem. Eng. Data Ser. 3 (1958) 263–272.

[4] T. Yuge, Experiments on heat transfer of spheres—report 3 (influence of free stream turbulence at higher Reynolds numbers), Rep. Inst. High Sp. Mech. Jpn. 11 (1959) 209–230.

[5] T. Yuge, Experiments on heat transfer of spheres, including combined natural and forced convection, J. Heat Transfer 82 (1960) 214–220.

[6] E. Venezian, M.J. Crespo, B.H. Sage, Thermal and material transfer in turbulent gas stream: one inch spheres, AIChE J. 8 (3) (1962) 383–388.

[7] T.R. Galloway, B.H. Sage, Thermal and material transfer in turbulent gas streams—a method of prediction for spheres, Int. J. Heat Mass Transfer 7 (1964) 283–291.

[8] T.R. Galloway, B.H. Sage, Thermal and material port from spheres. Prediction of macroscopic thermal and material transport, Int. J. Heat Mass Transfer 10 (1967) 1195–1210.

[9] W.J. Lavender, D.C. Pei, The effect of fluid turbulence on the rate of heat transfer from spheres, Int. J. Heat Mass Transfer 10 (1967) 529–539.

[10] G.D. Raithby, E.R.G. Eckert, The effect of turbulence parameters and support position on the heat transfer from spheres, Int. J. Heat Mass Transfer 11 (1968) 1233–1252.

[11] V.J. Gostkowski, F.A. Costello, The effect of free stream turbulence on heat and mass transfer from stagnation point of a sphere, Int. J. Heat Mass Transfer 13 (1970) 1382–1386.

[12] G.L. Hayward, D.C. Pei, Local heat transfer from a single spheres to a turbulent air stream, Int. J. Heat Mass Transfer 21 (1978) 35–41.

[13] J.G. Sandoval-Robles, H. Delmas, J.P. Couderc, Influence of turbulence on mass transfer between a liquid and a solid sphere, AIChE J. 27 (1981) 819–823.

[14] P.R. Yearling, Experimental determination of convective heat and mass transfer rates from single evaporating droplets in a turbulent air flow, Ph.D. Thesis, North Carolina State University, USA, 1995.

[15] G. Refai-Ahmed, M.M. Yovanovich, J.R. Culham, Experimental and approximate analysis of forced convection and isothermal spheres, J. Thermophys. Heat Transfer 11 (2) (1997) 223–231.

[16] I. Gökalp, C. Chauveau, O. Simon, X. Chesneau, Mass transfer from liquid fuel droplets in turbulent flow, Combust. Flame 89 (1992) 286–298.

[17] N. Hiromitsu, O. Kawaguchi, Influence of flow turbulence on the evaporation rate of suspended droplet in a hot air flow, Heat Transfer-Japanese Res. 24 (1995) 689–700.

[18] M. Birouk, C. Chauveau, B. Sarah, A. Quilgars, I. Gökalp, Turbulence effects on the vaporization of monocomponent single droplets, Combust. Sci. Technol. 113–114 (1996) 413–428.

[19] M. Birouk, I. Gökalp, A new correlation for turbulent mass transfer from liquid droplets, Int. J. Heat Mass Transfer 45 (2000) 37–45.

[20] J.-S. Wu, Y.-J. Lin, H.-J. Sheen, Effects of ambient turbulence and fuel properties on the evaporation rate of single droplets, Int. J. Heat Mass Transfer 44 (2001) 4593–4603.

[21] J.-S. Wu, K.-H. Hsu, P.-M. Kuo, H.-J. Sheen, Evaporation model of a single hydrocarbon fuel droplet due to ambient turbulence at intermediate Reynolds numbers, Int. J. Heat Mass Transfer 46 (2003) 4741–4745.

[22] J.-K Park, Droplet vaporization in turbulent flow, Ph.D. Thesis, University of Wisconsin-Madison, USA, 1987.

[23] M. Birouk, I. Gökalp, Current status of droplet evaporation in turbulent flows, Prog. Energy Combust. Sci. 32 (4) (2006) 408–423.

[24] M.M. Abou Al-Sood, M. Birouk, A numerical study of the effect of turbulence on mass transfer from a single fuel droplet evaporating in a hot convective flow, Int. J. Thermal Sci. 46 (2007) 779–789.

[25] M. Renksizbulut, M.C. Yuen, Numerical study of droplet evaporation in high temperature air stream, J. Heat Transfer 105 (1983) 384–388.

[26] M.M. Abou Al-Sood, M. Birouk, A numerical model for calculating the vaporization rate of a fuel droplet exposed to a convective turbulent airflow, Int. J. Numer. Meth. Heat Fluid Flow, in press.

[27] G.M. Faeth, Spray combustion phenomena, Proc. Combust. Inst. 26 (1996) 1593–1612.

[28] Y. Ohta, K. Shimoyama, S. Ohigashi, Bull. JSME 18 (1975) 47.

[29] N. Frössling, Gerl. Beitr. Geophys. 52 (1938) 170.

[30] M.M. Abou Al-Sood, A numerical study of a droplet evaporating in a turbulent airflow, Ph.D. Thesis, University of Manitoba, Canada, 2007.

[31] F.R. Menter, Two-equation eddy-viscosity turbulence models for engineering applications, AIAA J. 32 (8) (1994) 1598–1604.

[32] M. Birouk, M.M. Abou Al-Sood, Numerical study of sphere drag coefficient in turbulent flow at low Reynolds number, Numer. Heat Transfer Part A 51 (2007) 39–57.

[33] J.-R. Yang, S.-W. Wong, On the discrepancies between theoretical and experimental results for microgravity droplet evaporation, Int. J. Heat Mass Transfer 44 (2001) 4433–4443.

[34] C.C. Tseng, R. Viskanta, Effect of radiation absorption on fuel droplet evaporation, Combust. Sci. Technol. 177 (8) (2005) 1511–1542.

[35] P.L.C. Lage, R.H. Rangel, Single droplet vaporization including thermal radiation absorption, J. Thermophys. Heat Transfer 7 (3) (1993) 502–509.

[36] L.D. Karel, Recent experience with deferent turbulence models applied to the calculation of flow over aircraft components, Prog. Aerospace Sci. 34 (1998) 481–541.

[37] S.V. Patankar, Numerical Heat Transfer and Fluid Flow, Hemisphere Publishing Corporation, 1980.

[38] J.P. Van Doormall, G.D. Raithby, Enhancement of the simple method for predicting incompressible fluid flows, Numer. Heat Transfer 7 (1984) 147–163.

[39] H.-J. Leister, M. Perić, Vectorized strongly implicit solving procedure for a seven-diagonal coefficient matrix, Int. J. Numer. Meth. Heat Fluid Flow 4 (1994) 159–172.

[40] C.M. Megaridis, Comparison between experimental measurements and numerical predictions of internal temperature distributions of a

droplet vaporizing under high-temperature convective conditions, Combust. Flame 93 (1993) 287–302.

[41] S.-C. Wong, A.-C. Lin, Internal temperature distributions of droplets vaporizing in high-temperature convective flows, J. Fluid Mech. 237 (1992) 671–687.

[42] B. Abramzon, S. Sazhin, Droplet vaporization model in the presence of thermal radiation, Int. J. Heat Mass Transfer 48 (9) (2005) 1868–1873.

[43] H. Nomura, Y. Ujiie, H.J. Rath, J. Sato, M. Kono, Experimental study of high-pressure droplet evaporating using microgravity conditions, Proc. Combust. Inst. 26 (1996) 1267–1273.

[44] S.S. Sazhin, W.A. Abdelghaffar, E.M. Sazhina, M.R. Heikal, Models for droplet transient heating: effects on droplet evaporation, ignition, and break-up, Int. J. Thermal Sci. 44 (2005) 610–622.